

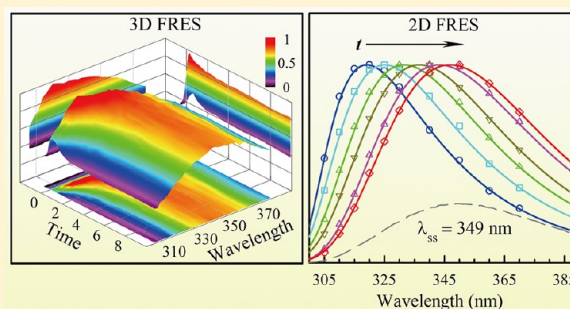
Validation of Response Function Construction and Probing Heterogeneous Protein Hydration by Intrinsic Tryptophan

Yangzhong Qin,[†] Chih-Wei Chang,^{†,‡} Lijuan Wang, and Dongping Zhong*

Department of Physics, Department of Chemistry and Biochemistry, and Programs of Biophysics, Chemical Physics, and Biochemistry, 191 West Woodruff Avenue, The Ohio State University, Columbus, Ohio 43210, United States

S Supporting Information

ABSTRACT: Protein solvation dynamics usually occur on multiple time scales with site specificity, and the characterization of such heterogeneous dynamics requires a convenient optical probe. We proposed a tryptophan methodology, and with site-directed mutagenesis we can use a tryptophan scan to probe any desirable position around protein surfaces. Here, we report our extended solvation model for construction of response functions for probes such as tryptophan with multiple emission peaks and lifetimes. We show our systematic construction procedure and careful analyses of the possible missing percentage of an initial ultrafast component with the established zero-time emission spectrum and limited temporal resolution through two methods of the direct mapping of femtosecond-resolved fluorescence spectra (3D FRES) and the constructed FRES (2D) from the fluorescence transients. We unambiguously validate our extended model with reexamination of solvation dynamics (methanol, water, and proteins) using conventional dye coumarin, intrinsic tryptophan, and cofactor flavin. Using mutant proteins of GB1, we show again the generality of the powerful probe tryptophan for protein hydration (solvation) and the slowdown of the hydration layer dynamics especially at the water–protein interface. These results justify the necessity of our extended solvation model, clarify the confusion of protein hydration in the recent literature, and establish the universal optical probe of tryptophan for heterogeneous protein dynamics.



I. INTRODUCTION

Solvation dynamics have been extensively studied in the past decades, both experimentally^{1–6} and theoretically,^{7–10} to understand the role of solvent on chemical reactions in polar and nonpolar solution.^{11,12} Typically, a dye molecule was excited in the solvent of interest, and a series of wavelength-resolved fluorescence transients from the blue to red side of the emission were taken to construct femtosecond-resolved fluorescence spectra (FRES). These spectra were fit with a standard log-normal function to extract the emission peaks. These time-dependent emission peaks, i.e., the Stokes shift with time, represent the energy relaxation of the probe due to solvent rearrangements induced by the sudden change of the dipole moment upon excitation, a dynamical evolution from the initial nonequilibrium configuration to the final relaxed equilibrium state. Under the linear-response approximation, the energy relaxation reflects the solvation dynamics of solvent fluctuations around the ground-state equilibrium. Thus, the solvation correlation function can be constructed and usually fit by multiple exponential decays. For most solvents, the initial decay is ultrafast in tens to a hundred of femtoseconds (fs), reflecting inertial, librational, and/or hindered rotational motions, followed by a mainly diffusive (translational) motion on the subpicosecond to picosecond (ps) time scales.^{1,2,13–15} However, such construction of correlation function becomes complicated when the solvation environment becomes

heterogeneous such as in proteins (not homogeneous like solvent solution), and the excited probe has multiple lifetimes with different emission peaks due to the dynamic heterogeneity of its conformation, one typical example of the intrinsic probe tryptophan widely used in protein dynamics.^{16–19}

We developed a methodology of using intrinsic tryptophan as an optical probe to study protein hydration dynamics ten years ago,^{17,20–23} and with site-directed mutagenesis we can place intrinsic tryptophan at any desirable location in a protein. We have systematically mapped out the global heterogeneous hydration dynamics around the surface of a globular protein apomyoglobin, directly observed the coupled water–protein fluctuations, and derived a series of correlations between hydrating water dynamics with protein chemical and structural properties, elucidating the dynamical nature of interfacial water molecules in hydration layers and their key roles on protein structure stability and flexibility.^{24–27} For protein solvation in the binding of active sites, we directly mapped out the FRES, not constructed, to derive correlation functions due to the complexity of emission spectra from the electrostatic and structural heterogeneity (constraints) at function sites.^{28,29} These developments have received significant attention, and the

Received: May 25, 2012

Revised: October 12, 2012

Published: October 17, 2012

results clearly showed the slowdown of water dynamics in protein hydration layers or function sites.¹⁹ Protein-associated water molecules (biological water) show very different dynamical behaviors from bulk water due to the interactions with proteins. Unfortunately, some recent work misinterpreted our methodology³⁰ and results,^{30–32} claiming similar ultrafast motions of biological water as in bulk water and that our method missed the huge initial ultrafast relaxation and that our observed slow solvation in tens of picoseconds is completely from protein relaxation. Also, we suggested several times before^{17,19,25,26} that, in view of controversies among MD simulations^{31,33–35} for the interpretation of the origin of slow relaxation as well as between simulation and experiment^{24–27} about the initial ultrafast relaxation and the assignment of slow relaxation, the integrity of the force field, the treatment of the water–protein interface, and the nature of nonequilibrium correlations be carefully scrutinized to directly compare with the experimental results.^{17,19}

In this report, we focus on the initial relaxation of the correlation function, and the slow solvation (hydration) in tens of picoseconds has been extensively addressed before.^{17,19,24–27} Here, we systematically analyze the methods for construction of solvation correlation functions from a homogeneous chemical solution of methanol and water buffer to heterogeneous protein environments of GB1 (B1 immunoglobulin-binding domain of protein G) mutants using dye coumarin, cofactor flavin, and intrinsic tryptophan as the optical probes, respectively. We construct the solvation correlation functions both from the wavelength- and fs-resolved fluorescence transients and from the direct mapping of FRES. With 300–400 fs resolution, we establish a procedure to determine the possible missing part of the initial ultrafast solvation components in tens to a hundred of femtoseconds. With the powerful intrinsic tryptophan, we unambiguously show the significant slowdown of the interfacial water dynamics in the hydration layers as demonstrated here again in the protein GB1. By these careful examinations, we validate our methodology of construction of correlation function using the intrinsic tryptophan probe and the slowdown of water dynamics in the hydration layers, show the generality of the powerful intrinsic tryptophan for probing protein hydration and dynamics, and clarify the recent confusion in the literature³⁰ on tryptophan methodology and related protein hydration.

II. EXPERIMENTAL SECTION

A. Sample Preparation. All chemicals of coumarin 152, coumarin 153, tryptophan (Trp), and flavin mononucleotide (FMN) were purchased from Sigma-Aldrich and used as received. The purification of GB1 protein has been described in detail elsewhere.³⁶ Two mutants reported here are double mutation of W43YN35W and W43YF30W. A mixture of coumarin 152 and 153 (50:50) with a dilute concentration of 5 μM was used. FMN was prepared at the concentration of 50 μM in 50 mM phosphate buffer solution at pH 7. Trp was dissolved in water with a concentration of 2–7 mM for experiment. The mutant protein concentration is about 2 mM in 10 mM Tris buffer solution at pH 7.5.

B. Femtosecond Methods. All the femtosecond-resolved measurements were carried out using the fluorescence up-conversion method. The experimental layout has been detailed elsewhere.^{28,37} Briefly, the pump wavelength was set at 400 nm for coumarin and FMN and at 280–295 nm for Trp, and its pulse energy typically was attenuated to ~ 140 nJ. The

instrument response time under the current noncollinear geometry is about 300–400 fs, and all data were taken at a magic angle (54.7°). All samples were kept in stirring or spinning quartz cells during irradiation to avoid heating and photobleaching. The time-resolved emission spectra at various delay times were obtained by scanning the mixing BBO angles and monochromator wavelengths simultaneously over the entire emission range. A variety of delay times were appropriately chosen to reconstruct the 3D FRES. The time zero at each wavelength was carefully calibrated. For wavelength-resolved fluorescence transients, we fixed the mixing BBO angle for each wavelength and measured the up-converted signal while scanning the pump-gating pulse delay time. Typically, we took a series of wavelength-resolved fluorescence transients from the blue end to the red side of the entire emission spectrum.

III. RESULTS AND DISCUSSION

A. Response Construction Procedure, Zero-Time Spectrum, and Solvation Correlation Function. The conventional solvation dynamics were typically studied by a fluorescent probe through a series of wavelength-resolved fluorescence transients taken from the blue- to red-side of the entire emission spectra. These transients were fit by a series of exponential decay components (typically 2 to 4) and then used to construct FRES to extract the fs-resolved emission peaks, $\nu(t)$, by fitting the spectra to a log-normal function. The final normalized solvation correlation function can be obtained as follows.⁶

$$C(t) = \frac{\nu(t) - \nu(\infty)}{\nu(0) - \nu(\infty)} \quad (1)$$

where $\nu(0)$ is a zero-time spectrum of a vibrationally relaxed lowest excited state (usually S_1 state) and should be independent of the excitation wavelength. The $\nu(0)$ value can be calculated by a model-independent method developed by Fee and Maroncelli,³⁸ which will also be used in this study. $\nu(\infty)$ is the final emission peak after the solvation is completed, and it is usually obtained from the steady-state spectrum. Practically, eq 1 is only valid under assumptions that (1) the fluorescence lifetime should be much longer than the solvation time scales, (2) the fluorescence probe should have only one population emission peak (mostly with one lifetime), usually set equal to the steady-state emission peak, and (3) the emission profile should follow a log-normal function; otherwise, the other parameters such as the average frequency^{1,28} ($\bar{\nu}$) will be used to replace the emission peak in eq 1. To extend eq 1 to the general case, we modified eq 1 to take care of assumptions (1) and (2) in the following.²¹

$$C(t) = \frac{\nu_s(t) - \nu_l(t)}{\nu_s(0) - \nu_l(0)} \quad (2)$$

where ν_s is the overall emission maximum including solvation dynamics and population decay contributions. ν_l is the total lifetime emission maximum due to the multiple population emission peaks with multiple lifetimes (typically with dynamic heterogeneous configurations). Typically, we assume that when the difference of $\nu_s - \nu_l$ reaches to 0.5 cm^{-1} the solvation dynamics is completed with the time of t_{sc} and the emission peak at ν_{sc} (typically slightly larger than the steady-state emission peak ν_{ss} , i.e., slightly bluer in wavelength).²¹ The total dynamic Stokes shift due to solvation is $\nu_s(0) - \nu_l(0)$. Note

that for the probe with only single lifetime emission, $\nu_i(t) = \nu_i(0) = \nu_i(\infty)$ and $\nu_s(t) = \nu(t)$, and eq 2 becomes eq 1. Here, we can separate the series of exponential decay components of the signal $I_\lambda(t)$ into the solvation and lifetime parts to construct the overall FRES and separated lifetime FRES to extract ν_s and ν_i .

$$I_\lambda(t) = I_\lambda^{\text{solv}}(t) + I_\lambda^{\text{popul}}(t) = \sum_i a_i e^{-t/\tau_i} + \sum_j b_j e^{-t/\tau_j} \quad (3)$$

where the first term is for solvation and the second term for lifetime emission. The coefficient a_i is positive (decay dynamics) at the blue side of the emission peak and is negative (initial rise) at the red side. The coefficient b_j is always positive and represents relative contributions of multiple lifetime emissions. With knowing the steady-state relative emission intensity I_λ^{ss} at λ , we can easily construct the FRES for the overall Stokes shift from eq 4 and the lifetime shift from eq 5 below.

$$I(\lambda, t) = \frac{I_\lambda^{\text{ss}} I_\lambda(t)}{\sum_i a_i \tau_i + \sum_j b_j \tau_j} \quad (4)$$

$$I^{\text{popul}}(\lambda, t) = \frac{I_\lambda^{\text{ss}} I_\lambda^{\text{popul}}(t)}{\sum_i a_i \tau_i + \sum_j b_j \tau_j} \quad (5)$$

Clearly, the “true” zero-time emission peak in eq 2 is critical and determines the total Stokes shift, i.e., total solvation energy. With typical temporal resolution of 300–400 fs in fluorescence detection by the up-conversion method, the initial ultrafast solvation in tens to a hundred of femtoseconds could be underestimated, and the constructed zero-time FRES could give a longer emission peak, a smaller $\nu_s(0)$ value. Here, we employed two methods to obtain the solvation dynamics and to estimate the zero-time spectrum. One is from the constructed FRES by the fluorescence transients using eqs 4 and 5, and the obtained zero-time emission peak $\nu_s(0)$ has been deconvoluted from the instrumental response. The other is from the directly measured FRES profile at zero pump–probe delay time ($t = 0$). This direct readout zero-time emission peak $\nu_s(0)$ is convoluted with the instrumental response and thus gives the lowest limit, i.e., the longest possible wavelength of the emission peak at zero time. The “true” zero-time peak or the constructed one from the fluorescence transients should shift to the blue side. With these considerations above, we first examined an equal mixture (50:50) of two coumarin dyes of C152 and C153 in methanol to examine how much the initial ultrafast component would be missed with such 300–400 fs resolution and then compared our results with those recently reported by the Petrich group,³⁰ and finally address the critical zero-time spectrum that could be different for measurements by various experimental methods. Coumarins 152 and 153 have their lifetimes of 0.9 and 4.0 ns with the steady-state emission peaks at 518 and 536 nm in methanol, respectively. Such the mixture system could mimic a dye probe with two lifetimes and two corresponding emission peaks, and thus the overall lifetime emission peak (ν_i) shifts with time. The steady-state emission peak of the mixture solution is at 534 nm, very close to C153's due to its dominant emission intensity (larger quantum yield). Thus, the lifetime emission shift (ν_i) is very small, 2 nm (70 cm^{-1}), which may not be an obvious example to demonstrate

the time-dependent $\nu_i(t)$, but we should still observe such lifetime emission shifting in eq 2.

Figure 1 shows the 3D FRES (top) directly obtained from scanning our spectrometry and the five typical fluorescence

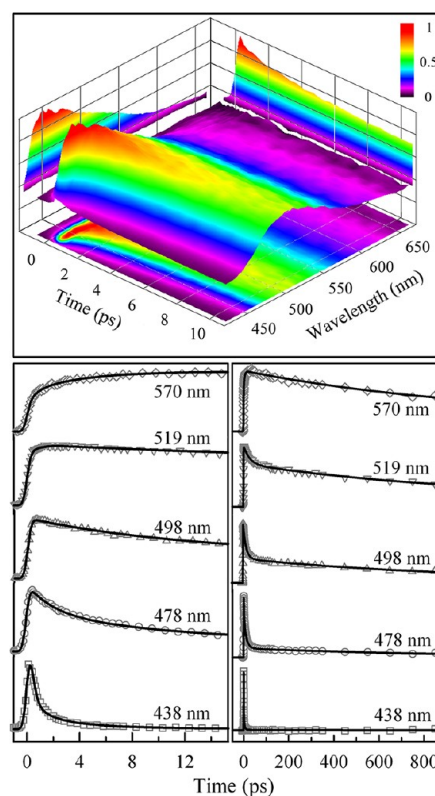


Figure 1. Solvation dynamics of a coumarin mixture (5 μM) of C152 and C153 (50:50) in methanol. The direct mapping of 3D FRES is shown at the top. The Raman scattering signal around 455 nm has been subtracted out. The several typical femtosecond-resolved fluorescence transients out of thirteen are shown at the bottom covering from the blue end to the red side of the entire emission spectrum. Note that at 438 and 478 nm the signals do not have any Raman scattering components.

transients (bottom) out of thirteen transients taken from the blue to red side of the emission with a time window of more than 3 ns. Note that the 438 nm transient is nearly at the blue end of the emission spectrum. For the blue-side transients, we need to use two solvation times (0.25–3.1 and 1.2–20 ps) and two lifetimes (0.9 and 4 ns) to fit the overall decay behavior. For example, at 438 nm, the transient was fit with 250 fs (87.7%) and 1.2 ps (11.9%). At the red side, we observed two initial rises (0.15–2.5 and 4.8–10.3 ps) besides two lifetime decays. We used a very dilute concentration of 5 μM (the same conditions as in ref 30), and thus a Raman scattering signal appears around 455 nm with 400 nm excitation. The 3D FRES has been subtracted out of the Raman scattering signal. Note that both transients at 438 and 478 nm have no Raman scattering components at all, as also confirmed by the transients taken at high concentrations to eliminate the Raman scattering signal, and thus the 438 nm transient at the blue end gives the fastest decay dynamics (250 fs) of solvation. The Raman-signal subtraction from the blue-side fluorescence transients at dilute concentrations is critical and directly affects the construction of FRES and the initial solvation time and amplitude.

In Figure 2A, we show the raw, direct FRES spectrum (blue curve) at 0.5 ps delay time, and clearly a Raman scattering

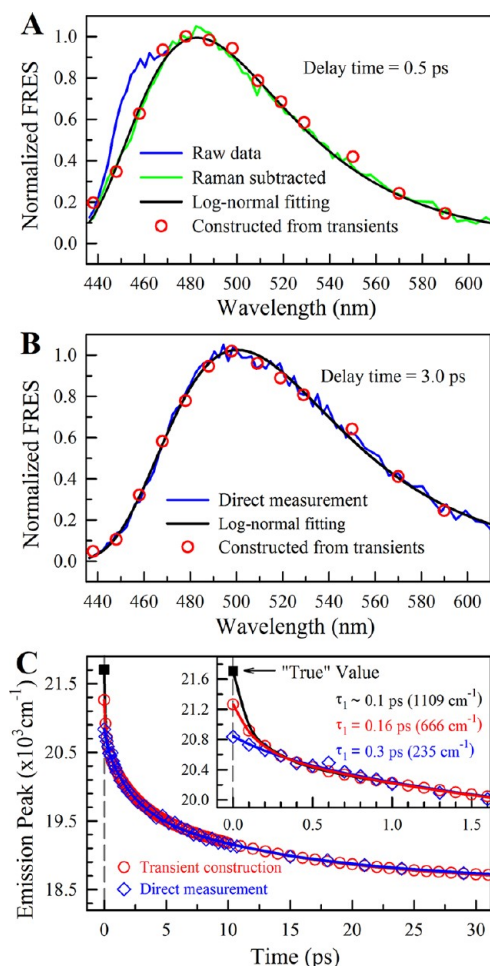


Figure 2. (A) Raw data (blue) from 3D FRES of the coumarin mixture in methanol at the delay time of 0.5 ps with the one by Raman subtraction (green). The red circles are constructed from the fluorescence transients also with the Raman subtraction at certain wavelengths. The black curve is the log-normal fitting. (B) Similar to (A) with the delay time of 3.0 ps. Note that at this delay time there is no Raman signal and the perfect match of direct (blue) and constructed (red) FRES signals. However, if the Raman subtractions in the fluorescence transients were not correct in the early delay time, the match with the direct FRES would not be good; see text. (C) The comparison of the obtained methanol relaxation dynamics with “true” time-zero spectral peak, the constructed and direct ones, showing the possible missing portions of the initial ultrafast components with the different methods.

signal around 455 nm appears on the shoulder at the blue side. Using a Gaussian function to represent the Raman signal and a log-normal function for the emission spectrum, we can perfectly fit the raw FRES, and the final emission spectrum after subtraction of the Raman signal (green curve) is also shown in Figure 2A with the log-normal fitting profile (black curve). Importantly, using the thirteen fluorescence transients with the Raman subtraction in three transients at 448, 458, and 468 nm, we constructed the FRES at 0.5 ps (red circles) using eq 4 and got results perfectly consistent with the direct FRES. To further examine if the Raman subtraction in the three transients is correct, we showed in Figure 2B the direct FRES (blue curve), the constructed FRES (red circles), and the fitting curve (black

curve) at a 3 ps delay time. It should be noted that both the direct FRES and the transients at 3 ps do not contain the Raman signals any more, and if the Raman signals were not subtracted correctly in the three transients at the shorter time, the constructed FRES from the transients at the longer time would not follow the log-normal profile. Thus, as shown in Figure 2B, we ensure that the Raman-signal subtraction in the three transients is correct, which enables all constructed FRES to be equal to the direct scanned FRES at the longer time.

Figure 2C shows the change of the FRES peaks with time $\nu_s(t)$, i.e., the solvation dynamics, by the two different methods of the directly scanned FRES and the constructed one from the fluorescence transients. Clearly, after 300–400 fs (our time resolution), the two derived curves (red and blue) are merged (inset in Figure 2C) to become nearly the same one. The derived zero-time spectrum peak is $\nu_0 = 21266 \text{ cm}^{-1}$ in the ν domain ($\lambda_0 = 463.8 \text{ nm}$ in the λ domain) from the constructed FRES and $\nu_0 = 20835 \text{ cm}^{-1}$ ($\lambda_0 = 475.3 \text{ nm}$) from the directly scanned FRES. As we mentioned earlier, due to the deconvolution of the transients from the instrument response, the derived zero-time spectrum from the constructed FRES is blue-shifted relative to that from the directly scanned FRES which has the longest wavelength for the zero-time spectrum peak without deconvolution. The “true” zero-time spectrum peak derived by the Fee–Maroncelli procedure was reported to be $\nu_0 = 21710 \text{ cm}^{-1}$.^{30,38} Thus, with three different initial values of ν_0 , we can fit the solvation dynamics with three different initial times of $\tau_1 \sim 0.1 \text{ ps}$ (1109 cm^{-1} from the “true” ν_0), 0.16 ps (666 cm^{-1} from the constructed FRES), and 0.3 ps (235 cm^{-1} from the direct FRES) besides another two solvation times of 2 ps (844 cm^{-1}) and 13 ps (1252 cm^{-1}). The “true” total Stokes shift is 3205 cm^{-1} , and the first component accounts for 34.6%. Due to our time resolution of $\sim 400 \text{ fs}$, using the construction method from the transients, we still missed 443 cm^{-1} , 40% of the first “true” component and 13.8% of the total solvation energy. Without deconvolution in the direct FRES, we missed 874 cm^{-1} , 78.8% of the first component and 27.3% of the total solvation energy. Thus, when the time resolution is much larger than the initial solvation time, the derived first solvation component will have an apparent longer dynamics and smaller solvation amplitude. Compared to the direct scanned FRES, the deconvolution of the transients recovers significantly more initial component with a shorter time scale and larger amplitude. To minimize the missing part, besides the time resolution, it is extremely important to obtain the fluorescence transient as at the blue end of the emission as possible; here we pushed the limit to take the transient at 438 nm. In the recent work by Petrich,³⁰ they took the blue-side transient only until 480 nm and derived $\nu_s(0) = 20120 \text{ cm}^{-1}$, compared with our $\nu_s(0) = 21266 \text{ cm}^{-1}$, and thus they missed 1590 cm^{-1} . In fact, they completely missed the first component (1109 cm^{-1}) and also more than half of the second component (481 cm^{-1}), leading to a huge missing initial component, 49% of the total solvation energy, and here we only missed 13.8%. Thus, Petrich et al.³⁰ missed half of the correlation function, which was not necessary with their resolution if they monitored much bluer fluorescence transients like at 438 nm here. We delay the discussion of $\nu_1(t)$ time behavior with other systems together until section C below.

To further examine the relationship of the time resolution with the missing initial ultrafast component, we did a series of simulations as shown in Figure 3. In Figure 3A, we assume a dye probe with two solvation times of $\tau_1 = 0.1 \text{ ps}$ (50%) and τ_2

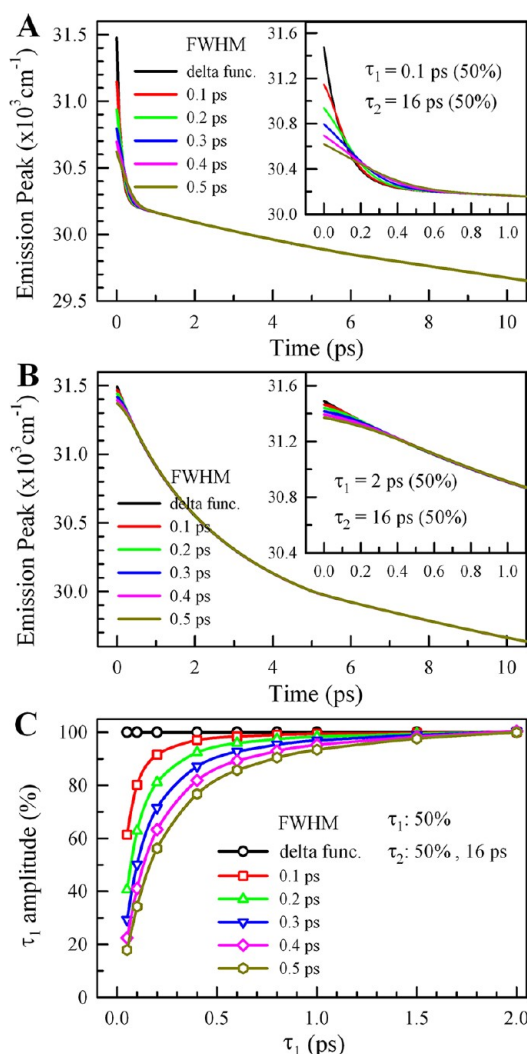


Figure 3. (A) Simulation of direct FRES with different temporal resolutions with a given solvation dynamics of 0.1 ps (50%) and 16 ps (50%). Note that the missing portions increase and the first apparent dynamics become slower when the temporal resolution gets larger (see inset). (B) A similar simulation as in (A) except that the first solvation time is changed to 2 ps. Note that the missing portions are minor (negligible) when the temporal resolution is shorter than the first solvation time. (C) The recovered percentage of the first direct FRES solvation component (50%) changes with the first solvation dynamics at different time resolutions. Note that the recovered percentage depends on the relative time scales between the first solvation dynamics and the temporal resolution.

= 16 ps (50%), having an initial zero-time peak $\nu_0 = 31\,476\text{ cm}^{-1}$, a final emission peak $\nu_\infty = 28\,996\text{ cm}^{-1}$, and a single lifetime of 3 ns. Thus, the emission peak $\nu_s(t)$ can be written as follows.

$$\nu_s(t) = (\nu_0 - \nu_\infty)[0.5e^{-t/0.1} + 0.5e^{-t/16}] + \nu_\infty \quad (6)$$

where t is in ps and the function is shown in the black curve in Figure 3A with the delta (δ) instrument response function (IRF). We assume that the emission spectra follow a log-normal function with a spectral width of 4400 cm^{-1} and an asymmetry factor of -0.1 . We first constructed a 3D FRES using eq 6 with a series of log-normal functions. Then, we cut the 3D FRES into a series of fs-resolved fluorescence transients at different wavelengths. We convoluted these transients with

different IRF (fwhm = 0.1–0.5 ps in Figure 3A) and then reconstructed new 3D FRES which have been convoluted with the different IRFs. We then cut these 3D FRES into a series of (2D) FRES at each fixed time (t) and fit these FRES with a log-normal function to extract $\nu_s(t)$. The derived results of $\nu_s(t)$ convoluted with the different IRFs (FWHMs) are shown in Figure 3A. Clearly, when the temporal resolution is larger than the first solvation dynamics (0.1 ps), the first component dynamics apparently becomes slower, and its amplitude gets smaller. At 0.5 ps resolution, the missing amplitude of the 0.1 ps solvation dynamics is as large as $\sim 65\%$ of the original percentage (50%). Similarly, we did another simulation with $\tau_1 = 2\text{ ps}$, keeping all other parameters the same, and the results are shown in Figure 3B. Although there are still some missing amplitudes with convolution of the IRFs, they are extremely minor and negligible because the temporal resolution (IRF) is much smaller than the initial solvation time (2 ps). Figure 3C summarizes the τ_1 amplitude percentage (of the original 50%) change with τ_1 at different temporal resolutions. Thus, for a given time resolution and the initial solvation dynamics, we can know the *maximum* missing percentage in Figure 3C. It should be emphasized here again that for the constructed FRES from the fluorescence transients with deconvolution from the IRF the missing percentage is significantly smaller, as demonstrated above in the coumarine C152/C153 mixture (Figure 2C). With the 78.8% missing part of the initial component and the time resolution of $\sim 400\text{ fs}$, the prediction of the initial solvation dynamics for the C152/C153 mixture, according to Figure 3C, is around 50–100 fs, consistent with the observed value ($\sim 100\text{ fs}$).^{6,39,40} For the case in Figure 3B, due to the slower initial solvation, the missing parts for both the direct and constructed FRES are not much different and are extremely small (negligible).

B. Intrinsic Probe Tryptophan, Redox Cofactor Flavin, and Biological Macromolecular Solvation. We have shown how to construct the solvation correlation function using the two different methods, direct and constructed, determine the longest zero-time spectrum peak from the direct FRES, and estimate the possible missing percentage given the limited time resolution and initial solvation dynamics. By knowing the “true” zero-time spectrum peak, we can know exactly how much will be missed for the initial part. For homogeneous bulk solvent, the solvation dynamics has been well characterized.⁶ However, for inhomogeneous biological systems, the solvation dynamics are complicated due to the heterogeneous environment, electrostatically and structurally, and the lack of a convenient, universal optical probe. We recently developed a tryptophan methodology^{21–23} and used intrinsic tryptophan as an optical probe.^{24–27,41–43} With site-directed mutagenesis, we can place tryptophan into any desirable location in a protein. We used a tryptophan scan, as demonstrated a universal probe and a powerful method,¹⁷ and mapped out the global hydration dynamics of a globular α -helical protein of apomyoglobin with 16 mutations.^{24,25} For the active or binding site of flavoproteins, we have used the native cofactor flavin as the optical probe and characterized the solvation dynamics at the several function sites of photolyase and flavodoxin.^{28,29} In the following, we characterize the probes of tryptophan (Trp) and flavin mononucleotide (FMN) in water or buffer solution.

Figure 4A shows the directly scanned 3D FRES with a Trp concentration of 7 mM at 290 nm excitation. At this concentration, we did not observe any noticeable Raman scattering signal around 321 nm under our excitation energy of

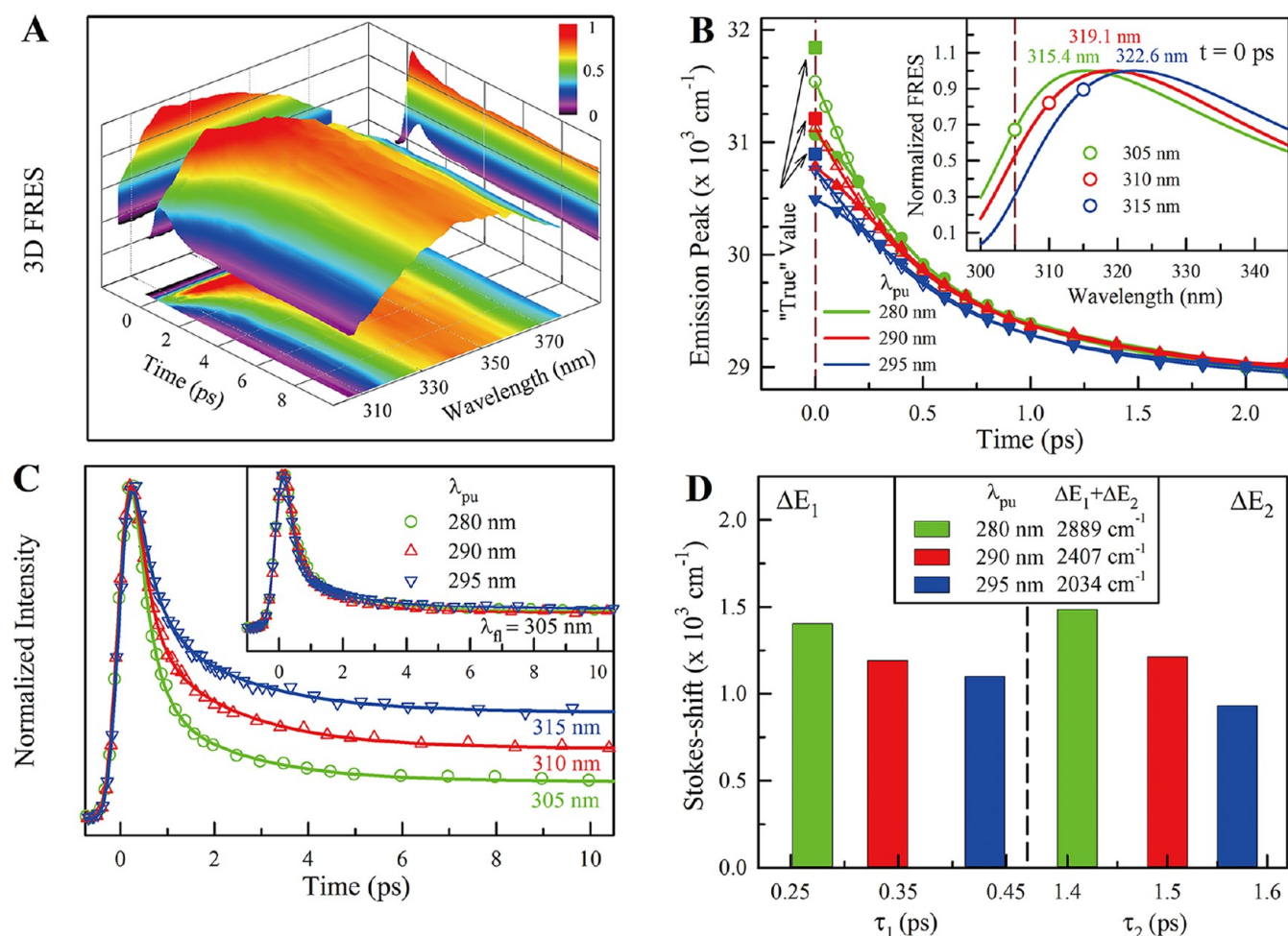


Figure 4. (A) Direct 3D FRES of tryptophan (7 mM) in bulk water at 290 nm excitation. At this concentration, no Raman signal was detected. (B) The obtained water relaxation dynamics from the direct (filled symbols) and constructed (unfilled symbols) FRES at three excitation wavelengths of 295, 290, and 280 nm. The "true" values (solid squares) are derived from the low-temperature data at 2 K. Inset: the constructed zero-time spectral peaks at three excitations. The dashed line marks 305 nm wavelength. (C) The fluorescence transients taken at 315, 310, and 305 nm at the similar separation from the emission peaks with three excitation wavelengths of 295, 290, and 280 nm, respectively, show the different ultrafast components. Inset: transients at 305 nm are nearly the same, but this wavelength has different separation from the emission peaks for three excitations; see text. (D) The obtained relaxation dynamics of tryptophan in bulk water with three different excitations and the corresponding relaxation energies. Clearly, the vibration relaxation occurs at 290 and 280 nm excitation; see text.

100–140 nJ. In Figure 4B, we show the final solvation dynamics from both the direct FRES (filled symbols) and constructed FRES (unfilled symbols) from the fluorescence transients (not shown) with three different excitation wavelengths at 280, 290, and 295 nm. The excitation at 295 nm is near the edge of the absorption, and we can basically assume that the vibrational relaxation upon excitation is minimal and the observed spectral shift is from the solvation Stokes shift. At 280 and 290 nm excitation, we can examine the degree of vibrational relaxation and the related relaxation time scales. Clearly, in Figure 4B, the constructed zero-time spectral peaks at 280, 290, and 295 nm excitation are 31 515, 31 141, and 30 754 cm⁻¹ with the corresponding wavelengths of 315.4, 319.1, and 322.6 nm (inset in Figure 4B), respectively. Correspondingly, the directly scanned zero-time peaks are at 31 046 (318.8 nm), 30 809 (321.43 nm), and 30 511 cm⁻¹ (324.5 nm). Interestingly, using the Fee–Maroncelli procedure³⁸ we found that the "true" zero-time spectrum is broadly structured with three peaks, not following a log-normal profile, and the strongest peak is very red, even longer than our constructed zero-time spectrum peak. Thus, we here take the strongest

emission peaks of low-temperature measurements at 2 K,⁴⁴ 31 840, 31 210, and 30 895 cm⁻¹ (extrapolated from the values at 300, 310, and 320 nm excitation), and the corresponding wavelengths at 312.2, 318.2, and 321.3 nm (filled squares in Figure 4B), as the "true" zero-time emission peaks for 280, 290, and 295 nm excitation, respectively. Thus, the corresponding maximum missing parts for the constructed spectral peaks are 325, 69, and 141 cm⁻¹. With these initial values, the total "true" spectral shifts are 3214, 2476, and 2175 cm⁻¹, and the constructed ones are 2889, 2407, and 2034 cm⁻¹, about 10%, 3%, and 6.5% missing energy of the total one. In the nonpolar solvent of cyclohexane, the emission peak at 290 nm excitation is around 312 nm, giving the upper limit for Trp in nonpolar environments. In the recent work by Petrich,³⁰ they reported the "true" zero-time spectral peak of 31 160 cm⁻¹ for NATA in water (did not mention what excitation wavelength was). The value is similar to our constructed one (31 141 cm⁻¹) at 290 nm excitation, still less than the one at 2 K.

Because the zero-time peaks at 290 and 280 nm are consecutively larger than that at 295 nm, moving to the bluer side, the vibrational relaxation at 290 and 280 nm excitation

occurs. Figure 4C shows the fluorescence transients gated at the roughly equal blue sides from the emission peaks (circles in inset in Figure 4B) for three excitations, and clearly the transient at 280 nm excitation shows the largest amplitude of the ultrafast component and then for 290 nm and at 295 nm the least ultrafast component. Also, we can compare the fluorescence transients at 305 nm (the dashed line in inset of Figure 4B and insert in Figure 4C) for three excitations, and clearly the similar three signals indicate that at 280 nm the transient has the largest ultrafast component because 305 nm is the closest to the zero-time emission peak and at 295 nm has the least due to being the farthest from the zero-time emission peak. Figure 4D shows the final results with the two relaxation time scales and the corresponding relaxation energies (note that the energies here have been subtracted out of the $\nu_1(t)$ part as discussed below). At 295 nm, the total solvation energy is about 2034 cm^{-1} , and thus at 290 nm the vibrational relaxation leads to an extra 373 cm^{-1} , about 18% of the total relaxation energy and close to the excitation energy gap of 585 cm^{-1} . However, at 280 nm, the vibrational relaxation results in an extra 855 cm^{-1} (29%), smaller than the excitation energy gap of 1816 cm^{-1} , reflecting that the difference of zero-time emission peaks is not equal to the excitation energy gap due to the different fluorescence transitions. The relaxation dynamics were fit with a double-exponential decay, but the first decay is stretched ($e^{-(t/\tau)^\beta}$) with β values of larger than 1 (~ 1.2) due to the nature of the initial Gaussian decay. For 295 nm excitation, the solvation dynamics are in 0.44 ps (54%) and 1.56 ps (46%); at 290 nm, the times become 0.34 ps (50%) and 1.5 ps (50%); and at 280 nm, they are 0.27 ps (49%) and 1.4 ps (51%). Clearly, the vibrational relaxation at 280 and 290 nm occurs on similar time scales of solvation from femtoseconds to 1–2 ps.⁴⁵

Figure 5A shows the direct scanned FRES for FMN in a buffer solution, and Figure 5B gives the final solvation dynamics from both constructed and direct FRES with the calculated “true” zero-time spectral peak by the Fee–Maroncelli procedure.³⁸ Since FMN does not dissolve in nonpolar solvent, we used a mixture of 1,4-dioxane (10%) and cyclohexane (90%) and obtained the “true” zero-time spectrum peak at 514.8 nm ($19\,187\text{ cm}^{-1}$). The actual “true” zero-time spectrum peak should be slightly bluer than 514.8 nm because 1,4-dioxane has a dielectric constant of 2.7. The constructed and direct zero-time spectral peaks are $19\,116$ and $18\,977\text{ cm}^{-1}$ and 516.4 and 519.8 nm , respectively. The total spectral shift is 826 cm^{-1} , and the constructed and direct ones are 766 and 637 cm^{-1} , resulting in 7.3% and 23.3% missing parts of the total energy, respectively. The solvation dynamics can be fit in three components. The first decay component is in 150 fs (320 cm^{-1}), 160 fs (233 cm^{-1}), and 500 fs (112 cm^{-1}) for the “true”, constructed, and directed spectral shifts, and the two other components are in 1.5 ps ($467\text{--}480\text{ cm}^{-1}$) and 11 ps ($40\text{--}53\text{ cm}^{-1}$).²⁹ Compared with Trp in water, the ratio of the total Stokes shifts of FMN to Trp is about 1:3, consistent with the ratio of dipole changes between the excited and ground states of the two molecules.²⁹ We noticed that a zero-time spectral peak of $\sim 21\,000\text{ cm}^{-1}$ and the Stokes shift of 2200 cm^{-1} for FMN in a protein were recently reported.⁴⁶ Clearly, this value was well overestimated by the inappropriate construction procedure.⁴⁶

With the careful characterization of Trp and FMN, we can integrate site-directed mutagenesis to examine a series of protein hydration/solvation around proteins and at active/

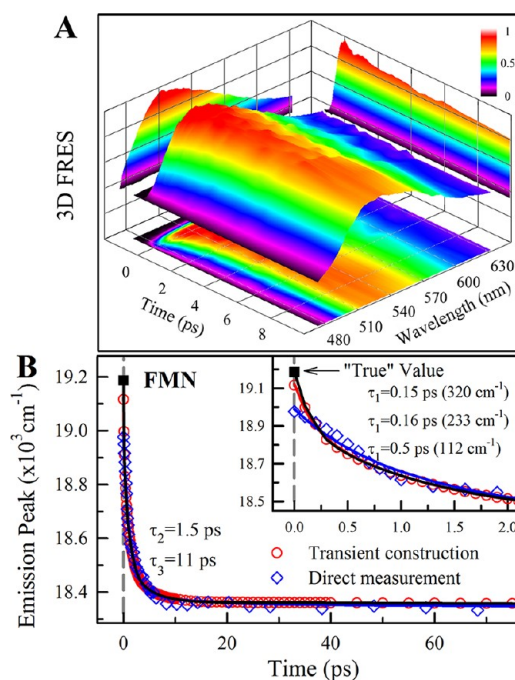


Figure 5. (A) Direct FRES for FMN ($50\text{ }\mu\text{M}$) in buffer solution. (B) The obtained relaxation dynamics from the “true” time-zero spectral peak, the constructed and direct ones, also showing the missing portions when the temporal resolution is longer than the initial solvation dynamics. Overall, the zero-time spectrum is relatively red, and the total Stokes shift is only about $700\text{--}800\text{ cm}^{-1}$; see text.

binding sites. The natural chromophore of GFP has also been used to study the protein solvation of variant GFP proteins.⁴⁷ Using the extrinsic dye labeling of proteins is very limited in general,^{48,49} and recently the synthetic amino acids as a potential probe have been incorporated to examine the electrostatic dynamics (solvation) in proteins.^{18,50} Various infrared probes,⁵¹ especially the $\text{--C}\equiv\text{N}$ group, can be powerful to examine various protein/enzyme dynamics as demonstrated recently.⁵² It is expected that the studies of protein dynamics including hydration/solvation will be rapidly advanced with new powerful probes and methodologies.

C. Lifetime Emission Shift, Biomolecular Heterogeneous Solvation, and Slowdown of Hydration Layer Dynamics. When the optical probe has multiple lifetimes (dynamical heterogeneity) with the different emission peaks, the overall lifetime emission peak, according to eq 5, shifts with time, $\nu_1(t)$. The derived overall spectral shift, ν_s , includes the contribution of ν_1 , and the difference, $\nu_s - \nu_1$, is the dynamic Stokes shift due to solvation. The correlation function can be calculated using eq 2. Figure 6 shows the typical ν_s and ν_1 distributions. We had showed the tryptophan case in our earlier report.²¹ In Figure 6A for the mixture of coumarins, it is clear that there is a spectral shift on the long time scale, although the amplitude is small. Because the solvation in water is ultrafast as for Trp, the lifetime shift can be easily separated from the solvation Stokes shift. However, when the relaxation time, especially in proteins, becomes significantly longer, the ν_1 cannot be ignored, and the ν_s decay does not follow obvious exponential behaviors. In Figure 6B and 6C, we show two relaxation dynamics of GB1 mutant proteins (N35W and F30W). One Trp emission peak is 352.4 nm with complete exposure to the surface water (polar environment), and the other one is 324.1 nm , which is buried in a more hydrophobic

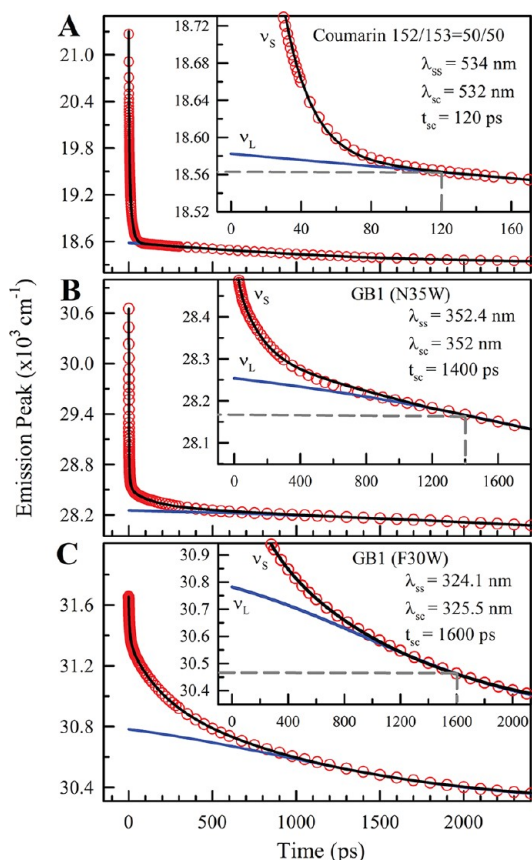


Figure 6. Total Stokes shifts ν_s and lifetime emission shifts ν_l for the coumarin mixture (A) and the GB1 mutant proteins of N35W (B) and F30W (C). Note that at the longer time the total relaxation behaviors do not follow the exponential decays due to the lifetime emission shift contribution, showing the critical subtraction of lifetime emission shift contribution.

protein environment. Clearly, the relaxation dynamics become longer, and the subtraction of the ν_l contribution is critical to determining the actual time scales and relaxation energies (see below). It was misleading and incorrect in the recent report³⁰ to state that eq 2 is not necessary for solvation response construction. It is obvious that as a general formula, as mentioned earlier, eq 2 covers all cases with either ultrafast or ultraslow solvation with multiple lifetime emission peaks. As shown in hydration/solvation of many proteins,^{24–27,41–43,53,54} the long-component solvation is expected, and eq 2 is essential to obtaining the correct response function. In Figure 6, the solvation complete times ($\nu_s - \nu_l = 0.5 \text{ cm}^{-1}$), τ_{sc} , are 120 ps for the mixture of coumarins, 1.4 ns for N35W, and 1.6 ns for F30W.

As we showed in mapping of global hydration dynamics of the globular apomyoglobin,^{24,25} the protein hydration highly depends on local chemical and structural properties. Thus, the protein hydration is very site specific and heterogeneous. We recently examined the global hydration dynamics of the mini-protein GB1 with more than 12 mutants. Here are shown two typical mutants with the extreme steady-state emission peaks of 352.4 and 324.1 nm, i.e., two environments of polar and hydrophobic (Figure 6B and 6C). For N35W, Figures 7A and 7B show the directly mapping 3D FRES and constructed FRES from the ten fluorescence transients, respectively. It should be emphasized that at 305 nm the fluorescence transient does not

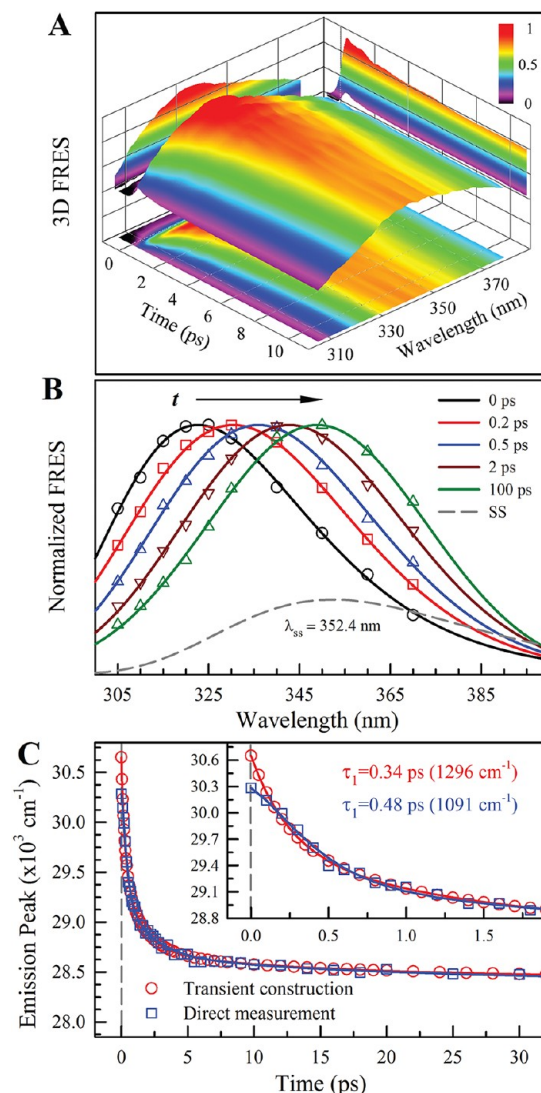


Figure 7. (A) Direct 3D FRES of the N35W mutant protein. (B) The constructed FRES from the ten fluorescence transients with a series of delay times. The dashed line is the steady-state emission spectrum with a peak at 352.4 nm. (C) The derived relaxation dynamics from the two methods of direct and constructed FRES, showing the closer dynamics and amplitudes of the two methods and indicating the missing portions very small ($\sim 20\%$ of the initial component from Figure 3C for the direct 3D FRES).

have any scattering or Raman signal and thus gives the fastest decay time (310 fs). Figure 7C reports the obtained relaxation dynamics by the two methods. The total Stokes shift is about 2397 cm^{-1} , similar to the value obtained in bulk water. The constructed zero-time emission peak is 322.7 nm, and the initial relaxation dynamics is 0.34 ps (1296 cm^{-1}), also similar to the values obtained in bulk water. The direct mapping zero-time peak is 327.8 nm, and the initial dynamics is 0.48 ps (1091 cm^{-1}). Thus, we might miss a very small portion of the initial ultrafast component as in bulk water. For F30W, Figures 8A and 8B show the direct 3D FRES and constructed FRES from the eight fluorescence transients, respectively. At 305 nm, we observed the fastest decay component in 5.2 ps, but at 330 nm we observed a rising component in 2.1 ps. We observed the zero-time emission peak at $\sim 313.6 \text{ nm}$ from both the direct and constructed methods, close to the values of Trp in nonpolar solvent and indicating a more hydrophobic environment. The

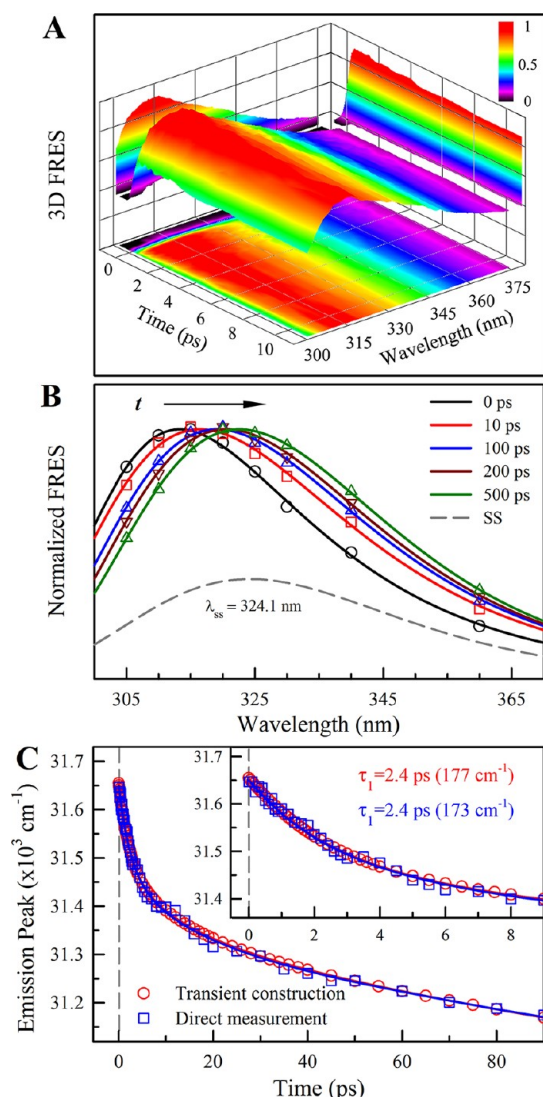


Figure 8. (A) Direct 3D FRES of F30W mutant protein. (B) Constructed FRES from the eight fluorescence transients with a series of delay times. The dashed line is the steady-state emission spectrum with a peak at 324.1 nm. (C) The derived relaxation dynamics from the two methods of direct and constructed FRES, showing the clear slowdown of the initial relaxation dynamics (2.4 ps). The two methods give the same initial times and amplitudes, indicating that there are nearly no missing portions of the initial components.

total Stoke shift is about 900 cm^{-1} . Figure 8C gives the obtained relaxation dynamics with the first relaxation dynamics in 2.4 ps. Both the methods give the same initial dynamics and similar amplitudes, indicating that the missing part is extremely small and negligible (Figure 3C).

Figure 9A shows the comparison of the fluorescent transients at 305 nm for Trp in water, N35W, and F30W GB1 mutant proteins at the same instrument conditions, and Figure 9B gives the correlation functions using eq 2. Clearly, the relaxation dynamics become slower in the proteins, especially for F30W mutant. In the fully exposed N35W, we observed four time scales of 0.34 (52%), 1.8 (31%), 16 (8%), and 222 ps (9%). The initial ultrafast component (0.34 ps) represents the nearly free water dynamics in the outer hydration layers, and the second fast component (1.8 ps) is from the water motions in the inner hydration layers at the water–protein interface. For the buried F30W, the three relaxation times were observed, 2.4

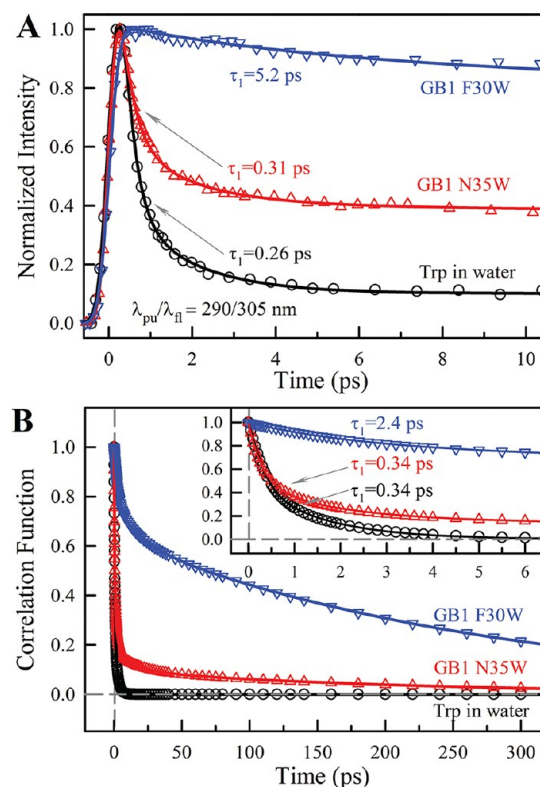


Figure 9. (A) Normalized, femtosecond-resolved fluorescence transients at 305 nm for three systems of Trp in water, N35W, and F30W mutant proteins under the same experimental conditions. The corresponding first decay components are in 0.26, 0.31, and 5.2 ps for the three systems, respectively. (B) The derived correlation functions from the constructed FRES for the three systems, clearly showing the slowdown of the protein hydration (solvation) at the water–protein interface; see text.

(21%), 16 (15%), and 275 ps (64%). Since the probe W30 is buried inside the protein, the initial relaxation dynamics of 2.4 ps represents the interfacial water dynamics in the inner hydration layers near the protein surface. Here, the W30 cannot detect the nearly free water molecules (ultrafast component) due to being far away from bulk water. As shown in our earlier studies by mutation of charged residues around the probe tryptophan,^{26,27} the dynamics in tens of picoseconds are the coupled water–protein relaxation, initially driven by the dominant water–network relaxation. The detailed hydration dynamics of globular mini-protein GB1 for more than ten mutants will be given elsewhere. Here, with systematic characterization of FRES and detailed construction of the response function, we unambiguously showed the correctness of eq 2 with careful analyses of the possible missing percentage of the initial ultrafast component. No doubt, the dynamics of solvation/hydration around protein surfaces slow down, especially at the interface between hydration water and the protein in a few picoseconds. The results here should clarify the recent confusion in the literature^{30–32} for misunderstanding eq 2 and erroneously claiming the ultrafast protein hydration/solvation and significant missing initial components. Also, we showed again here that for two mutant proteins the interfacial hydration dynamics clearly slows down, compared to bulk water.

IV. CONCLUSION

We reported our extended universal model for construction of solvation correlation function for dynamical heterogeneous probes with multiple emission peaks and lifetimes. With the limited time resolution, we carefully analyzed the possible missing percentage of the initial ultrafast component with two different methods of direct mapping of FRES and constructed FRES using the fluorescence transients. The direct FRES without deconvolution of the instrumental response gives the lowest limit of the zero-time spectral peak, and the constructed ones with deconvolution are closer to the “true” zero-time spectrum. The key issue is to take the fluorescence transient as at the blue end of the emission spectrum as possible to minimize the initial missing part. When the solvation dynamics is much shorter than the time resolution, we could miss some portion of the initial component, but when the dynamics is on the similar time scale (or longer) as the temporal resolution, the missing percentage could be minor and even negligible. We carefully reexamined several simple optical probes of dye coumarin, intrinsic tryptophan, and cofactor flavin and clarified the confusion in the recent literature³⁰ regarding our extended solvation model and tryptophan methodology. Using the powerful optical probe tryptophan with site-directed mutagenesis, we examined two mutant proteins of GB1 and showed again the necessity of the extended solvation model of eq 2 and the slowdown of the hydration layer dynamics at the interface between hydration water molecules and the protein surface.

■ ASSOCIATED CONTENT

■ Supporting Information

Complete reference 28. This material is available free of charge via the Internet at <http://pubs.acs.org>.

■ AUTHOR INFORMATION

Corresponding Author

*Phone: (614) 292-3044. Fax: (614) 292-7557. E-mail: zhong.28@asc.ohio-state.edu.

Present Address

[‡]Department of Chemistry, National Changhua University of Education, Changhua 50058, Taiwan.

Author Contributions

[†]These authors contributed equally.

Notes

The authors declare no competing financial interest.

■ ACKNOWLEDGMENTS

We thank Prof. Thomas Magliery (Ohio State University) for generously providing us the GB1 plasmid. Also thanks to Dr. Luyuan Zhang for the initial sample preparation of GB1 mutants and Jin Yang for the helpful discussion. This work was supported in part by the National Science Foundation (Grant CHE0748358) and the National Institute of Health (Grant GM095997).

■ REFERENCES

- (1) Maroncelli, M.; Fleming, G. R. *J. Chem. Phys.* **1987**, *86*, 6221–6239.
- (2) Kahlow, M. A.; Jarzeba, W.; Kang, T. J.; Barbara, P. F. *J. Chem. Phys.* **1989**, *90*, 151–158.
- (3) Fleming, G. R.; Cho, M. H. *Annu. Rev. Phys. Chem.* **1996**, *47*, 109–134.

- (4) Stratt, R. M.; Maroncelli, M. *J. Phys. Chem.* **1996**, *100*, 12981–12996.
- (5) Glasbeek, M.; Zhang, H. *Chem. Rev.* **2004**, *104*, 1929–1954.
- (6) Horng, M. L.; Gardecki, J. A.; Papazyan, A.; Maroncelli, M. *J. Phys. Chem.* **1995**, *99*, 17311–17337.
- (7) Maroncelli, M. *J. Mol. Liq.* **1993**, *57*, 1–37.
- (8) Hsu, C. P.; Song, X. Y.; Marcus, R. A. *J. Phys. Chem. B* **1997**, *101*, 2546–2551.
- (9) Cramer, C. J.; Truhlar, D. G. *Chem. Rev.* **1999**, *99*, 2161–2200.
- (10) Tomasi, J.; Mennucci, B.; Cammi, R. *Chem. Rev.* **2005**, *105*, 2999–3093.
- (11) Maroncelli, M.; Macinnis, J.; Fleming, G. R. *Science* **1989**, *243*, 1674–1681.
- (12) Barbara, P. F.; Walker, G. C.; Smith, T. P. *Science* **1992**, *256*, 975–981.
- (13) Jimenez, R.; Fleming, G. R.; Kumar, P. V.; Maroncelli, M. *Nature* **1994**, *369*, 471–473.
- (14) Carter, E. A.; Hynes, J. T. *J. Chem. Phys.* **1991**, *94*, 5961–5979.
- (15) Stratt, R. M.; Cho, M. H. *J. Chem. Phys.* **1994**, *100*, 6700–6708.
- (16) Pal, S. K.; Zewail, A. H. *Chem. Rev.* **2004**, *104*, 2099–2123.
- (17) Zhong, D. *Adv. Chem. Phys.* **2009**, *143*, 83–149.
- (18) Cohen, B. E.; McAnaney, T. B.; Park, E. S.; Jan, Y. N.; Boxer, S. G.; Jan, L. Y. *Science* **2002**, *296*, 1700–1703.
- (19) Zhong, D.; Pal, S. K.; Zewail, A. H. *Chem. Phys. Lett.* **2011**, *503*, 1–11.
- (20) Zhong, D.; Pal, S. K.; Zhang, D. Q.; Chan, S. I.; Zewail, A. H. *Proc. Natl. Acad. Sci. U.S.A.* **2002**, *99*, 13–18.
- (21) Lu, W. Y.; Kim, J.; Qiu, W. H.; Zhong, D. *Chem. Phys. Lett.* **2004**, *388*, 120–126.
- (22) Zhang, L. Y.; Kao, Y. T.; Qiu, W. H.; Wang, L. J.; Zhong, D. *J. Phys. Chem. B* **2006**, *110*, 18097–18103.
- (23) Qiu, W. H.; Li, T. P.; Zhang, L. Y.; Yang, Y.; Kao, Y. T.; Wang, L. J.; Zhong, D. *Chem. Phys.* **2008**, *350*, 154–164.
- (24) Zhang, L. Y.; Wang, L. J.; Kao, Y. T.; Qiu, W. H.; Yang, Y.; Okobiah, O.; Zhong, D. *Proc. Natl. Acad. Sci. U.S.A.* **2007**, *104*, 18461–18466.
- (25) Zhang, L. Y.; Yang, Y.; Kao, Y. T.; Wang, L. J.; Zhong, D. *J. Am. Chem. Soc.* **2009**, *131*, 10677–10691.
- (26) Qiu, W. H.; Kao, Y. T.; Zhang, L. Y.; Yang, Y.; Wang, L. J.; Stites, W. E.; Zhong, D.; Zewail, A. H. *Proc. Natl. Acad. Sci. U.S.A.* **2006**, *103*, 13979–13984.
- (27) Qiu, W. H.; Wang, L. J.; Lu, W. Y.; Boechler, A.; Sanders, D. A. R.; Zhong, D. *Proc. Natl. Acad. Sci. U.S.A.* **2007**, *104*, 5366–5371.
- (28) Chang, C. W.; et al. *Proc. Natl. Acad. Sci. U.S.A.* **2010**, *107*, 2914–2919.
- (29) Chang, C. W.; He, T. F.; Guo, L. J.; Stevens, J. A.; Li, T. P.; Wang, L. J.; Zhong, D. *J. Am. Chem. Soc.* **2010**, *132*, 12741–12747.
- (30) Bose, S.; Adhikary, R.; Mukherjee, P.; Song, X. Y.; Petrich, J. W. *J. Phys. Chem. B* **2009**, *113*, 11061–11068.
- (31) Nilsson, L.; Halle, B. *Proc. Natl. Acad. Sci. U.S.A.* **2005**, *102*, 13867–13872.
- (32) Halle, B.; Nilsson, L. *J. Phys. Chem. B* **2009**, *113*, 8210–8213.
- (33) Golosov, A. A.; Karplus, M. *J. Phys. Chem. B* **2007**, *111*, 1482–1490.
- (34) Li, T. P.; Hassanali, A. A.; Kao, Y. T.; Zhong, D.; Singer, S. J. *J. Am. Chem. Soc.* **2007**, *129*, 3376–3382.
- (35) Toptygin, D.; Woolf, T. B.; Brand, L. *J. Phys. Chem. B* **2010**, *114*, 11323–11337.
- (36) Bao, W. J.; Gao, Y. G.; Chang, Y. G.; Zhang, T. Y.; Lin, X. J.; Yan, X. Z.; Hu, H. Y. *Protein Expression Purif.* **2006**, *47*, 599–606.
- (37) Saxena, C.; Sancar, A.; Zhong, D. *J. Phys. Chem. B* **2004**, *108*, 18026–18033.
- (38) Fee, R. S.; Maroncelli, M. *Chem. Phys.* **1994**, *183*, 235–247.
- (39) Shiota, H.; Pal, H.; Tominaga, K.; Yoshihara, K. *J. Phys. Chem.* **1996**, *100*, 14575–14577.
- (40) Gustavsson, T.; Cassara, L.; Gulbinas, V.; Gurzadyan, G.; Mialocq, J. C.; Pommeret, S.; Sorgius, M.; van der Meulen, P. *J. Phys. Chem. A* **1998**, *102*, 4229–4245.

- (41) Qiu, W. H.; Zhang, L. Y.; Kao, Y. T.; Lu, W. Y.; Li, T. P.; Kim, J.; Sollenberger, G. M.; Wang, L. J.; Zhong, D. *J. Phys. Chem. B* **2005**, *109*, 16901–16910.
- (42) Qiu, W. H.; Zhang, L. Y.; Okobiah, O.; Yang, Y.; Wang, L. J.; Zhong, D.; Zewail, A. H. *J. Phys. Chem. B* **2006**, *110*, 10540–10549.
- (43) Kim, J.; Lu, W. Y.; Qiu, W. H.; Wang, L. J.; Caffrey, M.; Zhong, D. *J. Phys. Chem. B* **2006**, *110*, 21994–22000.
- (44) Scott, T. W.; Campbell, B. F.; Cone, R. L.; Friedman, J. M. *Chem. Phys.* **1989**, *131*, 63–79.
- (45) Bram, O.; Oskouei, A. A.; Tortschanoff, A.; van Mourik, F.; Madrid, M.; Echave, J.; Cannizzo, A.; Chergui, M. *J. Phys. Chem. A* **2010**, *114*, 9034–9042.
- (46) Chosrowjan, H.; Taniguchi, S.; Mataga, N.; Phongsak, T.; Sucharitakul, J.; Chaiyen, P.; Tanaka, F. *J. Phys. Chem. B* **2009**, *113*, 8439–8442.
- (47) Abbyad, P.; Childs, W.; Shi, X. H.; Boxer, S. G. *Proc. Natl. Acad. Sci. U.S.A.* **2007**, *104*, 20189–20194.
- (48) Lang, M. J.; Jordanides, X. J.; Song, X.; Fleming, G. R. *J. Chem. Phys.* **1999**, *110*, 5884–5892.
- (49) Bose, S.; Adhikary, R.; Barnes, C. A.; Fulton, D. B.; Hargrove, M. S.; Song, X. Y.; Petrich, J. W. *J. Phys. Chem. A* **2011**, *115*, 3630–3641.
- (50) Abbyad, P.; Shi, X. H.; Childs, W.; McAnaney, T. B.; Cohen, B. E.; Boxer, S. G. *J. Phys. Chem. B* **2007**, *111*, 8269–8276.
- (51) Waegle, M. M.; Culik, R. M.; Gai, F. *J. Phys. Chem. Lett.* **2011**, *2*, 2598–2609.
- (52) Jha, S. K.; Ji, M. B. A.; Gaffney, K. J.; Boxer, S. G. *Proc. Natl. Acad. Sci. U.S.A.* **2011**, *108*, 16612–16617.
- (53) Peon, J.; Pal, S. K.; Zewail, A. H. *Proc. Natl. Acad. Sci. U.S.A.* **2002**, *99*, 10964–10969.
- (54) Pal, S. K.; Peon, J.; Zewail, A. H. *Proc. Natl. Acad. Sci. U.S.A.* **2002**, *99*, 1763–1768.